Soft modes and superconductivity in the layered hexagonal carbides V_2CAs, Nb_2CAs, and Nb_2CS

S. V. Halilov,[1,2] D. J. Singh,[1] and D. A. Papaconstantopoulos[1]
[1]*Center for Computational Materials Science, Naval Research Laboratory, Washington, DC 20375*
[2]*Department of Materials Science and Engineering, University of Pennsylvania, Philadelphia, Pennsylvania 19104*
(Received 14 December 2001; revised manuscript received 19 February 2002; published 29 April 2002)

The electronic structure, selected phonon frequencies, and electron phonon coupling of the hexagonal layered compounds Nb_2CS, Nb_2CAs, and V_2CAs are elucidated using density functional calculations. All materials are good three-dimensional metals with moderate values of the density of states, $N(E_F)$. The electronic structure of Nb_2CS, the only superconductor within this family of materials, consists of well-hybridized Nb $d-S$ $p-C$ p derived bands characteristic around the Fermi energy. The S is more ionic in this compound than the As in the related arsenides Nb_2CAs or V_2CAs. This results in a relative softness for phonon modes involving S. Rigid muffin tin approximation calculations show moderate electron phonon couplings consistent with low-temperature superconductivity. The key difference from the carbo-arsenides is the presence of soft moderately coupled S modes.

DOI: 10.1103/PhysRevB.65.174519 PACS number(s): 74.25.Jb, 71.20.Lp

I. INTRODUCTION

Sakamaki and co-workers recently reported the discovery of novel carbosulfide superconductors.[1–3] These are based on Nb_2CS, which has a critical temperature $T_c \approx 5$ K and occurs in the layered ''H'' (also known as ''MAX'') phase structure,[4,5] as shown in Fig. 1. This hexagonal structure consists of rocksaltlike MX, separated by intervening $A=$Al, Ga, In, Tl, Si, Ge, Sn, Pb, P, As or S layers. The weakness of the bonding through the A layers coupled with relatively strong transition-metal carbide and nitride layers is thought to underlie the potentially useful mechanical properties observed in some of these phases. This has been the focus of most of the recent work on these materials.[5,6]

The structural motif, however, bears some similarity to the borocarbide and boronitride family of superconductors like $LuNi_2B_2C$ and $La_3Ni_2B_2N_3$.[7–9] That family shows a maximum T_c of 23 K and is characterized by sheets of Ni, Pd, or Pt closely coordinated by B, with intervening rocksaltlike rare-earth carbide or nitride layers. In those materials, superconductivity is understood to arise from an electron-phonon mechanism, related to a high density of states (DOS) at the Fermi energy E_F, $N(E_F)$, and high deformation potentials associated with the transition-metal ligand bonding.[10–15] Interestingly, the electronic structures are quite three dimensional despite the layered appearance of the crystal structures. Turning to the ''H'' phases, most have not been studied from the point of view of superconductivity. Sakamaki and co-workers note that C and S have similar electronegativities and speculate that this may underlie the interesting properties of this material.

Some related phases have been investigated at the density functional level including Ti_2AlC, Ti_2AlN, Ti_3AlC_2, Ti_3AlN_2, and Ti_3SiC_2 with emphasis on mechanical properties.[16–19] Here we use such calculations to elucidate the high-temperature superconducting prospects in the ''H'' phases. To our knowledge, no superconductivity has been found experimentally in either V_2CAs or Nb_2CAs, which can best be understood in terms of the lattice stiffness (Sec. II).

The electronic structure and related properties of Nb_2CS relevant to superconductivity in relation to Nb_2CAs and V_2CAs, are derived within the local density approximation[20] (LDA) in Sec. III. The Schrödinger equation is solved using the general potential linearized augmented plane-wave (LAPW) method[21,22] with well-converged basis sets and Brillouin zone samplings. Electron-phonon interactions were then determined from the LAPW results within the rigid muffin tin approximation (RMTA) of Gaspari and Gyorffy[23,24] (Sec. IV).

II. CRYSTAL STRUCTURE, BOND CHARACTERISTICS, AND RAMAN FREQUENCIES

The synthesis and crystal structures of V_2CAs and Nb_2CAs were reported more than 30 years ago.[25,26] The

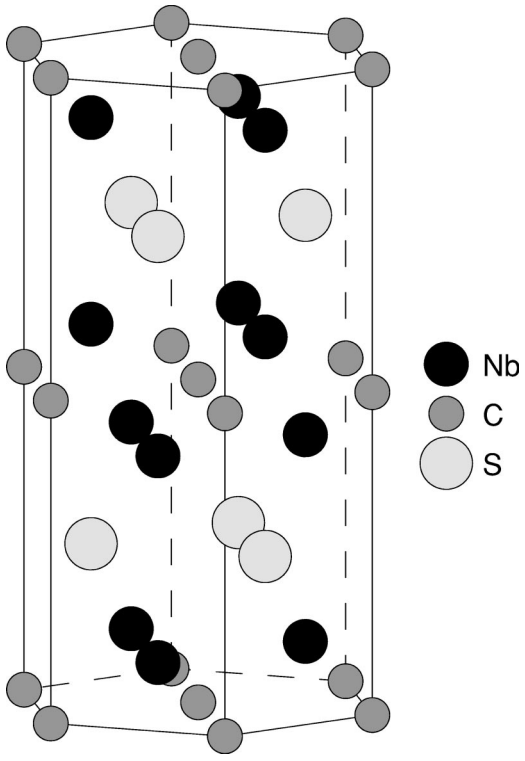

FIG. 1. Hexagonal layered structure of Nb_2CS.

compounds occur with space group $P6_3/mmc$. There are two formula units per cell. The structure consists of hexagonal C sheets that are coordinated above and below by transition-metal sheets. These are arranged so the C is octahedrally coordinated by metal atoms. These M_2C units are separated by As or S sheets, which are much further from M than the C. The coordination of the As(S) is trigonal prismatic, which results in the hcp-like stacking of the M_2C subunits. The crystal structure has one free internal parameter, denoted $z(M)$. This defines the height of the M atoms above the C sheets, i.e., the distortion of the edge sharing CM_6 octahedra. Ideal octahedra are most favorable for C $2p$-M d σ bond formation—presumably an important ingredient in the stability of the compounds—while lower heights favor direct M-M hopping between the two M sheets in a M_2C subunit. This may be expected to be of importance due to the small size of the C atom. It should also be noted that there may be significant M d-A p interactions, A = As, S, based on the larger size of A relative to C. Note that there is a competition of bonding interactions in this structure, so the insertion of larger atoms into the A site leads to more covalency. The M-A distance is also controlled by $z(M)$.

The experimental crystal structures yield, for Nb_2CAs, $a = 3.317$ Å and $c = 11.90$ Å, with $z(\mathrm{Nb}) = 0.098$, and for V_2CAs, $a = 3.113$ Å and $c = 11.38$ Å, with $z(\mathrm{V}) = 0.086$.[25,26] Within this structure the V-V distance in V_2CAs is less than in bulk V, which is odd. A similar structure of Nb_2CS was determined by Sakamaki and co-workers,[1] using x-ray diffraction, with the lattice parameters $a = 3.294$ Å and $c = 11.552$ Å. No doubt, the measured diffraction values of a and c are more reliable than what can be obtained by density functional calculations, and so we use these values.

On the other hand, $z(M)$, which plays an important role in determining the electronic structure, has been varied during the calculations, both to obtain a more reliable value of this parameter than could be determined from experiment and to get information about the corresponding Raman phonon. In this way, we obtained $z(\mathrm{Nb}) = 0.0942$, $z(\mathrm{Nb}) = 0.0952$, and $z(\mathrm{V}) = 0.0907$ with the calculated Raman phonon frequencies at this coordinate of 273 cm^{-1}, 270 cm^{-1}, and 340 cm^{-1} for Nb_2CAs, Nb_2CS, and V_2CAs, respectively. Only little anharmonicity is associated with the motion of $z(M)$, which is clearly seen from Fig. 2, where the calculated energy vs $z(\mathrm{Nb})$ is well fit by a quadratic.

Thus, it turns out that the A_g Raman frequencies in Nb_2CAs and Nb_2CS are practically identical, which, however, does not necessarily mean that their lattice stiffnesses are close. The difference can be readily understood in terms of the bond lengths and bond character.

With the calculated structure, the CM_6 octahedra are compressed along z in all compounds. The in-plane Nb-Nb distance in Nb_2CAs is 3.32 Å, while the interlayer Nb-Nb distance is 2.95 Å. For comparison, the Nb-Nb distance in bulk Nb metal is 2.86 Å. As such, direct Nb-Nb hopping between the two Nb layers in the Nb_2C subunits should be anticipated. The Nb-C distance is 2.22 Å, which is slightly

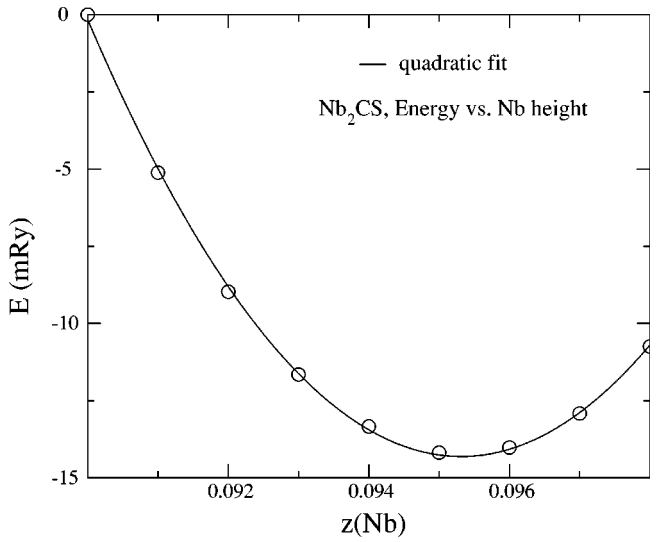

FIG. 2. Relative energy as a function of Nb position $z(\mathrm{Nb})$ in Nb_2CS.

less than in bulk NbC. Thus strong hopping via C should also be expected. If the octahedra were perfect, this would only couple Nb orbitals on atoms in opposing sheets, but here there is a significant compression, which would permit in-plane hopping via C p orbitals as well. The Nb-As distance is 2.36 Å. The corresponding bond lengths in V_2CAs follow a similar pattern, with one exception. That is, even though V is a smaller ion than Nb, the V-As distance is larger than the Nb-As. In particular it is 2.55 Å. This probably reflects the in-plane compression of the As sheets due to the smaller a lattice parameter. As noted by Barsoum,[5] based on crystallographic trends in this family, the a lattice parameter is controlled almost entirely by the MX interactions, where here $X = \mathrm{C}$.

Proceeding with the analysis of the lattice stiffness, we notice that, in particular, the full symmetry A_g is a motion of the Nb atoms against the C sheet, to which they are close. The smaller nearest-neighbor Nb-C bond length with the calculated $z(\mathrm{Nb})$ in Nb_2CS suggests a slightly stronger Nb-C interaction (perhaps unexpected considering the higher electron count) and weaker Nb-S interaction compared to the Nb-As interaction in Nb_2CAs. To check this we calculated two other zone center phonons for both materials. These were the phonons corresponding to C and S motions with the two slabs in the unit cell moving in phase. This was done by calculating atomic forces on the atoms with several small displacements of the atoms consistent with this symmetry, and then setting up (by fitting) and diagonalizing the resulting dynamical matrix. For Nb_2CAs, we obtained a mode at 255 cm^{-1} consisting of As moving against the Nb_2C trilayer and a mode at 540 cm^{-1} consisting of C motion against the coordinating Nb octahedra. For Nb_2CS, the corresponding modes are at 261 cm^{-1} and 520 cm^{-1}, indicating a very similar stiffness for the Nb_2C trilayers, but a much softer lattice for S motion relative to As (N.B. $m_s/m_{\mathrm{As}} \approx 0.43$, so the similar frequency implies a much softer lattice). As discussed below, this is a result of the ionic character of the S interaction with the Nb_2C trilayers.

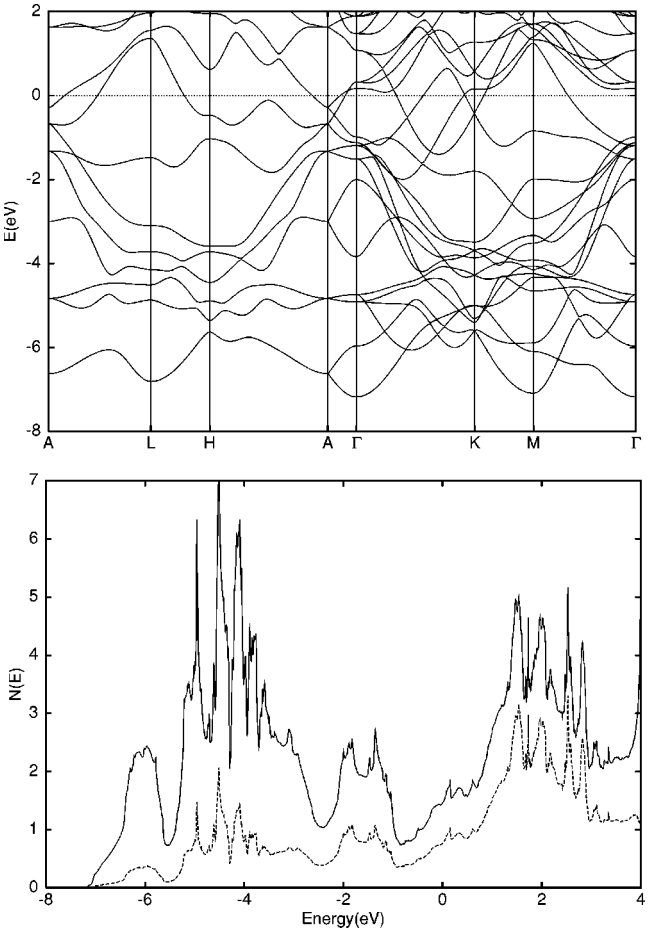

FIG. 3. LDA band structure (top) and electronic DOS (bottom) of Nb_2CAs using the calculated value of the internal structural parameter, $z(\mathrm{Nb})=0.0942$. The DOS is on a per formula unit (half unit cell) basis. The solid line is the total DOS and the dashed line is the Nb *d* projection on the LAPW spheres, again on a per formula unit basis. The zero is at E_F.

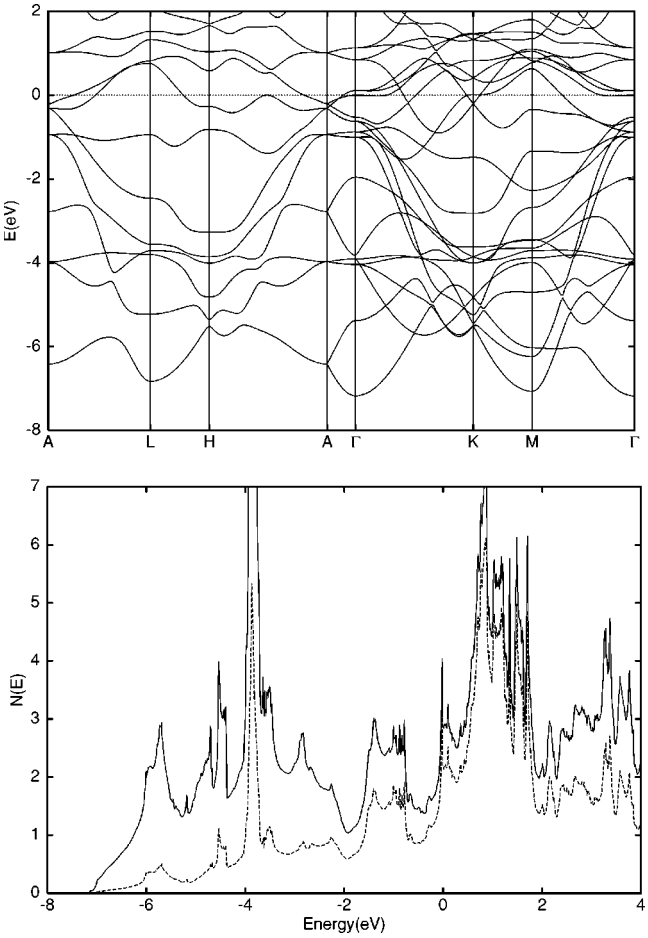

FIG. 4. LDA band structure (top) and DOS (bottom) of V_2CAs using the calculated value of the internal structural parameter, $z(\mathrm{V})=0.0907$, as in Fig. 3. The dashed line in the DOS is the V *d* projection. The zero is at E_F.

III. ELECTRON STRUCTURE

A. Nonsuperconducting carbides Nb_2CAs and V_2CAs

The calculated band structures and densities of states are shown in Figs. 3 and 4, for Nb_2CAs and V_2CAs, respectively. Not surprisingly, the *d* bands are more narrow in the V compound. However, the basic features of the Nb_2CAs and V_2CAs band structures are similar. The valence bands may be roughly described as consisting of a broad background of dispersive ligand derived bands on top of which there are narrower transition-metal *d* bands. Both of these compounds show a peak in the DOS near -4 eV. This arises from σ bonding combinations of C *p* and *M d*, which yield six bonding bands (three per C atom corresponding to the three *p* orbitals). The corresponding six antibonding states are 2–4 eV above E_F, in the uppermost manifold of crystal field split *d* bands. Also against this background there are more *d*-derived states. These are split into a peak centered around -1 eV (this may also be described as hybridized As p–M *d* states) and a larger more pure *d*-derived peak centered at 1 eV or 2 eV (for the V and Nb compounds, respectively). As may be expected, based on consideration of the generally less extended $3d$ as opposed the $4d$ orbitals, the DOS peaks are narrower and stronger in the V compound while the crystal field splitting is higher in the Nb compound.

In Nb_2CAs, E_F falls in the pseudogap due to the *M d* crystal field. This region is dominated by dispersive high-velocity bands of mixed character. In particular, the band structures show large dispersion in the k_z direction, as seen along Γ-*A*. In the hexagonal crystal structure, the $k_z=0.5$ plane [(*A*-*L*-*H*-*A*) in the band plots] has higher symmetry than $k_z=0$. In particular, the bands are at least twofold degenerate at $k_z=0.5$. They split into symmetric and antisymmetric combinations at $k_z=0$. These splittings indicate the size of the *c*-axis interactions.

In V_2CAs, the crystal field splitting is smaller than in Nb_2CAs and as a result flat *d*-derived bands are present at E_F, leading to the peak in the DOS near E_F. The flatness is particularly pronounced in a region around Γ as may be seen from the Γ-*M* and Γ-*K* dispersions near E_F. This is somewhat analogous to the situation in $LuNi_2B_2C$, where some parts of the zone have flat Ni *d*-derived bands near E_F, although in the present case the DOS peak is considerably lower. We obtain $N(E_F)=2.9\ \mathrm{eV}^{-1}$ per formula unit in

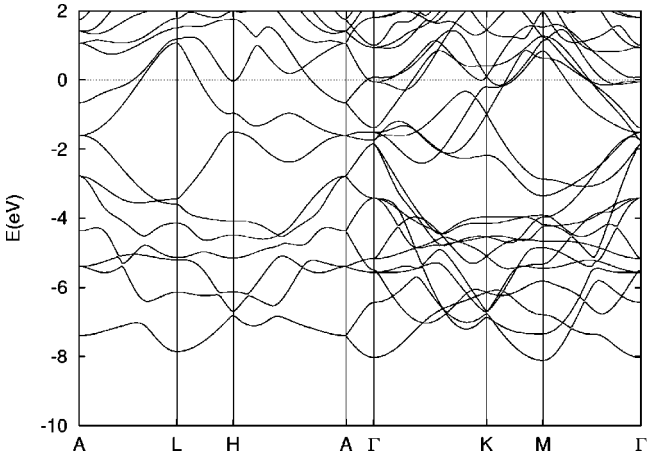

FIG. 5. LDA band structure of Nb_2CS using the calculated value of $z(\mathrm{Nb})=0.0952$. The energy zero is at E_F.

V_2CAs, as compared with $N(E_F)=4.8\ \mathrm{eV}^{-1}$ in $LuNi_2B_2C$, also per two transition-metal atoms.[11] The value for Nb_2CAs is much lower, $N(E_F)=1.5\ \mathrm{eV}^{-1}$. Fixed spin moment calculations were done for V_2CAs to check for a magnetic instability, but none was found.

B. Superconducting carbide Nb_2CS

The calculated LDA band structure of Nb_2CS is shown in Fig. 5. The corresponding electronic DOS and projections are given in Fig. 6. The bands near E_F are given to a reasonable approximation by a rigid band shift of the Fermi level of Nb_2CAs, corresponding to the two extra valence electrons per cell. Despite the higher Fermi energy, E_F remains in the same manifold of dispersive bands. This region of the band structure lies in a pseudogap between two prominent peaks in the DOS. The lower one, from ≈ -8 eV to -2 eV, comes from C p and S p states and the upper one from Nb d states. The C p states are, however, quite strongly hybridized with the Nb d orbitals, and so part of the lower peak, especially from -8 eV to -5 eV, is better described as C p–Nb d σ bonding combinations. The upper peak, starting just above E_F and extending to ≈ 5 eV, formally contains the corresponding antibonding combinations. Sakamaki and co-workers in their experimental reports mention the similar electronegativity of C and S. This similarity is reflected in the band structure, in the sense that the nominal C and S bands are occupied and occur nearby in the band structure. However, the similarities stop there. As might be anticipated from the bonding topology, the S is much more weakly hybridized with Nb than the C, with very little S character appearing in the Nb derived peak above E_F. Comparing with the DOS for Nb_2CAs, it is also seen that the S in Nb_2CS is more ionic than the As in that material, which no doubt underlies the softer S force constant reflected in the phonons, as discussed above.

The Fermi energy falls in the pseudogap region just below the Nb d peak onset. Here the electronic states are hybridized mixtures of Nb d C p and S p states. The calculated total DOS at E_F for Nb_2CS is 2.9 eV^{-1} on a per unit cell basis, which is essentially the same as the value for Nb_2CAs.

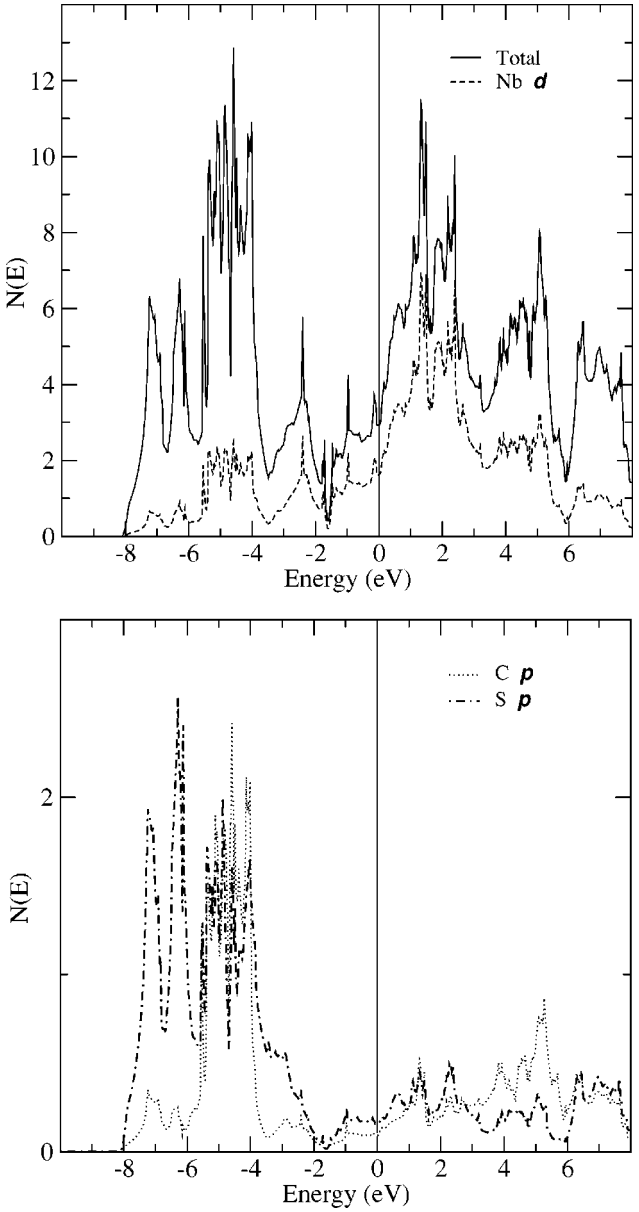

FIG. 6. Calculated total and projected electronic DOS of Nb_2CS. The DOS and projections are on a per unit cell basis. The top panel shows the total DOS and the Nb d projection, while the bottom shows the ligand p projections. The energy zero is at E_F.

IV. ELECTRON-PHONON COUPLING AND SUPERCONDUCTIVITY

Within the usual BCS electron-phonon theory,[27,28] the couplings are given by $\lambda=\eta/\langle m\omega^2\rangle$, where $\eta=N(E_F)\times\langle g_{ep}^2\rangle_{FS}$ is the McMillan-Hopfield parameter, g_{ep} stands for the matrix element of the electron-ion interaction, and $\langle m\omega^2\rangle$ is an average force constant characterizing the phonons. Thus, depending on the electronic structure, the relative softness of the S vibrations relative to As, as discussed in Sec. I, could potentially play a role in the superconductivity of Nb_2CS.

The electron-phonon coupling was evaluated on the basis

TABLE I. RMTA McMillan-Hopfield and related parameters for Nb_2CS, Nb_2CAs, and V_2CAs. $N_s(E_F)$, $N_p(E_F)$, $N_d(E_F)$, and $N_f(E_F)$ are the *s*, *p*, *d*, and *f* DOS projected onto each LAPW sphere, on a per atom basis (states/Ry/spin); $N_s^{(1)}$, $N_p^{(1)}$, $N_d^{(1)}$, and $N_f^{(1)}$ are the corresponding free scatter DOS as defined in the Gaspari-Gyorffy theory; δ_s, δ_p, δ_d, and δ_f are the scattering phase shifts; and η_{sp}, η_{pd}, and η_{df} are the contributions to η (eV/Å^2) for each site for the corresponding scattering channel. E_F and $N(E_F)$ used in Eq. (1) were 0.877 Ry and 19.9 $Ry^{-1}spin^{-1}$ for Nb_2CS, 0.854 Ry and 19.8 $Ry^{-1}spin^{-1}$ for Nb_2CAs, and 0.808 Ry and 39.15 $Ry^{-1}spin^{-1}$ for V_2CAs.

	Nb_2CS			Nb_2CAs			V_2CAs		
	Nb	C	S	Nb	C	As	V	C	As
r_{mt}	2.20	1.55	2.20	2.20	1.55	2.20	2.20	1.55	2.20
$N_s(E_F)$	0.01	0.02	0.08	0.01	0.01	0.06	0.02	0.01	0.09
$N_p(E_F)$	0.02	0.32	0.53	0.03	0.36	0.64	0.05	0.38	0.76
$N_d(E_F)$	2.75	0.04	0.23	2.59	0.04	0.11	7.37	0.07	0.14
$N_f(E_F)$	0.03	0.01	0.01	0.03	0.00	0.01	0.03	0.01	0.03
$N_s^{(1)}$	0.11	0.19	0.14	0.11	0.20	0.19	0.17	0.20	0.19
$N_p^{(1)}$	0.16	1.56	1.31	0.15	1.58	1.30	0.23	1.64	1.35
$N_d^{(1)}$	6.39	0.02	0.37	6.46	0.02	0.18	13.92	0.02	0.16
$N_f^{(1)}$	0.02	0.00	0.02	0.02	0.00	0.02	0.01	0.00	0.01
δ_s	-1.13	0.99	1.04	-1.12	1.00	0.77	-0.81	1.04	0.83
δ_p	-0.51	1.17	1.43	-0.50	1.15	0.84	-0.24	1.13	0.88
δ_d	1.35	0.01	0.12	1.26	0.01	0.04	-1.47	0.01	0.04
δ_f	0.01	0.00	0.00	0.01	0.00	0.00	0.00	0.00	0.00
η_{sp}	0.00	0.00	0.01	0.00	0.00	0.00	0.00	0.00	0.00
η_{pd}	0.05	0.32	0.20	0.07	0.35	0.13	0.04	0.32	0.11
η_{df}	0.73	0.00	0.01	0.69	0.00	0.00	0.83	0.00	0.00
η	0.79	0.32	0.23	0.76	0.35	0.13	0.88	0.32	0.11

of the RMTA calculations.[23] Within this approximation η is given by

$$\eta = \frac{E_F N(E_F)}{\pi^2} \sum_l \frac{2(l+1)\sin^2(\delta_{l+1}-\delta_l)}{N_l^{(1)} N_{l+1}^{(1)}} n_l n_{l+1}, \quad (1)$$

where δ_l is the scattering phase shift at the Fermi energy E_F and angular momentum l, and $N_l^{(1)}$ is the single-scatterer DOS which, as defined in Ref. 23, is an integral involving the radial wave functions. $n_l \equiv N_l / N(E_F)$ are the fractional DOS expressed in terms of N_l, the angular momentum components of the DOS inside the muffin-tin spheres, and $N(E_F)$, the per spin DOS at E_F.

Details of the ionic McMillan-Hopfield parameters and the parameters entering the Gaspari-Gyorffy theory are given in Table I. We find that the largest McMillan-Hopfield parameters η are on the metallic site in all ''H''-carbide systems in question. Here we obtain $\eta_{Nb}=0.79$ eV/Å^2, $\eta_{Nb}=0.76$ eV/Å^2, and $\eta_V=0.88$ eV/Å^2 per ion, whereas the total η factors are 4.1 eV/Å^2, 4.0 eV/Å^2, and 4.4 eV/Å^2 for Nb_2CS, Nb_2CAs, and V_2CAs, respectively.

Note that the η factors are nearly the same in all systems, although the density of states $N(E_F)$ is twice as big in the V-contained carbide than in the Nb-contained carbides. This is obviously because the squared matrix element of the electron-phonon interaction averaged over the Fermi surface, $\langle g_{ep}^2 \rangle_{FS}$, is essentially smaller in V-contained carbide. The outer-shell electrons are spatially more contracted around the V site ($3d$ element) than around the Nb site ($4d$ element), which makes the V sites rather ionic and efficiently leads to a much weaker shift-induced interaction between V and C from the adjacent layer than that between Nb and C. The coupling on C is smaller than for Nb or V and similar for all materials, while the contribution from the As sites is much smaller.

To assess the electron-phonon coupling λ in binary carbides and related compounds, it is often a good approximation to set $\langle m\omega^2 \rangle$ equal for all atoms.[24] For a nearest-neighbor central force model, this simply reflects Newton's laws. Using this approximation and using a normal value of $\mu^*=0.13$ for the Coulomb pseudopotential in the McMillan-Dynes equation for T_c,[27,28] we find that to obtain any superconductivity above 1 K, the average phonon frequency would have to be less than 160 cm^{-1} and 233 cm^{-1} for Nb_2CAs and V_2CAs, respectively. These values seem unreasonably low for compounds from a class of structural materials, especially considering the calculated values of the full symmetry Raman active phonon mode. Thus, while superconductivity is not excluded, it does not seem likely that either Nb_2CAs or V_2CAs will form the basis of high-temperature electron-phonon superconductors analogous to the borocarbides and boronitrides.

However, unlike the carbo-arsenides there is a significant contribution from S in Nb_2CS, $\eta_S=0.23$ eV/Å^2 per ion, as compared to $\eta_{As}=0.13$ eV/Å^2 or $\eta_{As}=0.11$ eV/Å^2 for carbo-arsenides. This, combined with the weaker S bonding of Nb_2CS, may be the key difference from carbo-arsenides for superconductivity. To make a simple estimate, we take the three *z* direction phonon frequencies, mentioned above, as representative of the bonding of S, Nb, and C, respectively. This yields a value of $\langle m\omega^2 \rangle$ more than 3 times higher for Nb than for S (and approximately twice higher for C). According to this crude estimate, the contribution to λ from S will be approximately half the Nb contribution (note that there are 4 Nb and only 2 S in the unit cell), while the As contribution in carbo-arsenides is negligible. If this is correct, then the total λ for Nb_2CS would be 50% higher than in carbo-arsenides. On the other hand, there is no reason to suppose that the phonon frequencies themselves are significantly different between the carbo-sulfide and carbo-arsenides, in which case the prefactor of the McMillan-Dynes equation would be the same for the two materials. We speculate that this reason, i.e., coupling on the S site, is responsible for the superconductivity of Nb_2CS.

Finally, we comment on the prospects for obtaining high values of T_C in the ''H'' phases. Rigid muffin tin calculations of the electron-phonon interaction indicate only modest coupling, which is not favorable for superconductivity at elevated temperatures.

ACKNOWLEDGMENTS

We thank D.U. Gubser for suggesting this problem. This work was supported by ONR and the the ASC supercomputer center.

[1] K. Sakamaki, H. Wada, H. Nozaki, Y. Onuki, and M. Kawai, Solid State Commun. **112**, 323 (1999).
[2] K. Sakamaki, H. Wada, H. Nozaki, Y. Onuki, and M. Kawai, Mol. Cryst. Liq. Cryst. Sci. Technol., Sect. A **341**, 99 (2000).
[3] K. Sakamaki, H. Wada, H. Nozaki, Y. Onuki, and M. Kawai, Solid State Commun. **118**, 113 (2001).
[4] H. Nowotny, Prog. Solid State Chem. **2**, 27 (1970).
[5] M.W. Barsoum, Prog. Solid State Chem. **28**, 201 (2000).
[6] M.W. Barsoum and T. El-Raghy, Am. Sci. **89**, 334 (2001).
[7] R. Nagarajan, C. Mazumdar, Z. Hossain, S.K. Dhar, K.V. Gopalakrishnan, L.C. Gupta, C. Godart, B.D. Padalia, and R. Vijayaraghavan, Phys. Rev. Lett. **72**, 274 (1994).
[8] R.J. Cava, H. Takagi, B. Batlogg, H.W. Zandbergen, J.J. Krajewski, W.F. Peck, Jr., R.B. van Dover, R.J. Felder, T. Siegrist, K. Mizuhashi, J.O. Lee, H. Eisaki, S.A. Carter, and S. Uchida, Nature (London) **367**, 146 (1994).
[9] R.J. Cava, H.W. Zandbergen, B. Batlogg, H. Eisaki, H. Takagi, J.J. Krajewski, W.F. Peck, Jr., E.M. Gyorgy, and S. Uchida, Nature (London) **372**, 245 (1994).
[10] L.F. Mattheiss, Phys. Rev. B **49**, 13 279 (1994).
[11] W.E. Pickett and D.J. Singh, Phys. Rev. Lett. **72**, 3702 (1994).
[12] D.J. Singh, Phys. Rev. B **50**, 6486 (1994).
[13] L.F. Mattheiss, T. Siegrist, and R.J. Cava, Solid State Commun. **91**, 587 (1994).
[14] D.J. Singh and W.E. Pickett, Phys. Rev. B **51**, 8668 (1995).
[15] D.J. Singh and W.E. Pickett, Nature (London) **374**, 682 (1995).
[16] A.L. Ivanovskii and N.I. Medvedeva, Mendeleev Commun. **9**, 36 (1999).
[17] N.I. Medvedeva, D.L. Novikov, A.L. Ivanovsky, M.V. Kuznetsov, and A.J. Freeman, Phys. Rev. B **58**, 16 042 (1998).
[18] Z. Sun and Y. Zhou, Phys. Rev. B **60**, 1441 (1999).
[19] Y. Zhou and Z. Sun, Phys. Rev. B **61**, 12 570 (2000).
[20] L. Hedin, and B.I. Lundqvist, J. Phys. C **4**, 2064 (1971).
[21] D.J. Singh, *Planewaves, Pseudopotentials and the LAPW Method* (Kluwer Academic, Boston, 1994).
[22] D. Singh, Phys. Rev. B **43**, 6388 (1991).
[23] G.D. Gaspari and B.L. Gyorffy, Phys. Rev. Lett. **29**, 801 (1972).
[24] B.M. Klein and D.A. Papaconstantopoulos, Phys. Rev. Lett. **32**, 1193 (1974).
[25] H. Boller and H. Nowotny, Monatsch. Chem. **97**, 1053 (1966).
[26] O. Beckmann, H. Boller, and H. Nowotny, Monatsch. Chem. **99**, 1580 (1968).
[27] W.L. McMillan, Phys. Rev. **167**, 331 (1968).
[28] R.C. Dynes, Solid State Commun. **10**, 615 (1972).